Ebrahimi *et al.*
Journal of Analytical Science and Technology (2022) 13:10
https://doi.org/10.1186/s40543-022-00318-5

Journal of Analytical Science and Technology

RESEARCH ARTICLE Open Access

Rapid and efficient colorimetric sensing of clindamycin and Fe^{3+} using controllable phyto-synthesized silver/silver chloride nanoparticles by *Syzygium cumini* fruit extract

Atefeh Ebrahimi[1], Fayezeh Samari[1,2*], Ebrahim Eftekhar[3] and Saeed Yousefinejad[4]

Abstract: The first evidence of a green, single-step, and additive-free process for the fabrication of silver/silver chloride nanoparticles (Ag/AgCl NPs) by fruit extract of *Syzygium cumini* (*S. cumini*) without the usage of any stabilizer and halide source was provided. The formation of nanoparticles was optimized to control the shape, size, and stability via various pHs of the reaction mixture, the quantity of fruit extract, temperature, concentrations of silver ion, and reaction time. The optimal conditions were determined: pH = 7.0, the quantity of the leaf extract = 3.0 mL, silver ion concentration = 1.0 mM, temperature = 60 °C, and incubation time = 40 min. As an application in colorimetric sensing, the ability of the prepared Ag/AgCl NPs to sense clindamycin and Fe^{3+} ion in an aqueous medium was investigated. The SPR band and color of the solution of Ag/AgCl NPs undergo dramatic changes in exposure to clindamycin with new SPR peaks appearing at 500 nm, accompanied by a color change from yellow to pink due to the aggregation of NPs. Under the optimized pH of 3.0, this sensor was shown a linear dynamic range from 10.0 to 100.0 μM with a LOD of 1.2 μM and good linear relationships ($R^2 = 0.99$) for clindamycin. On the other hand, the quenching of the SPR peak at 412 nm was used to monitor the Fe^{3+} ions with wide linear ranges of 10.0–350.0 μM under the optimized pH (pH = 9) with a LOD of 5.6 μM. In addition, the proposed sensor displayed applicability in the real sample containing clindamycin (in capsules and injection ampoules) and Fe^{3+} ions (in water samples) detection.

Keywords: Ag/AgCl nanoparticles, Plant extract, Colorimetric sensor, Spectrometry, Iron ion

*Correspondence: fsamari@hormozgan.ac.ir
[1] Department of Chemistry, Faculty of Sciences, University of Hormozgan, P.O. Box 3995, Bandar Abbas, Iran
Full list of author information is available at the end of the article

Graphical Abstract

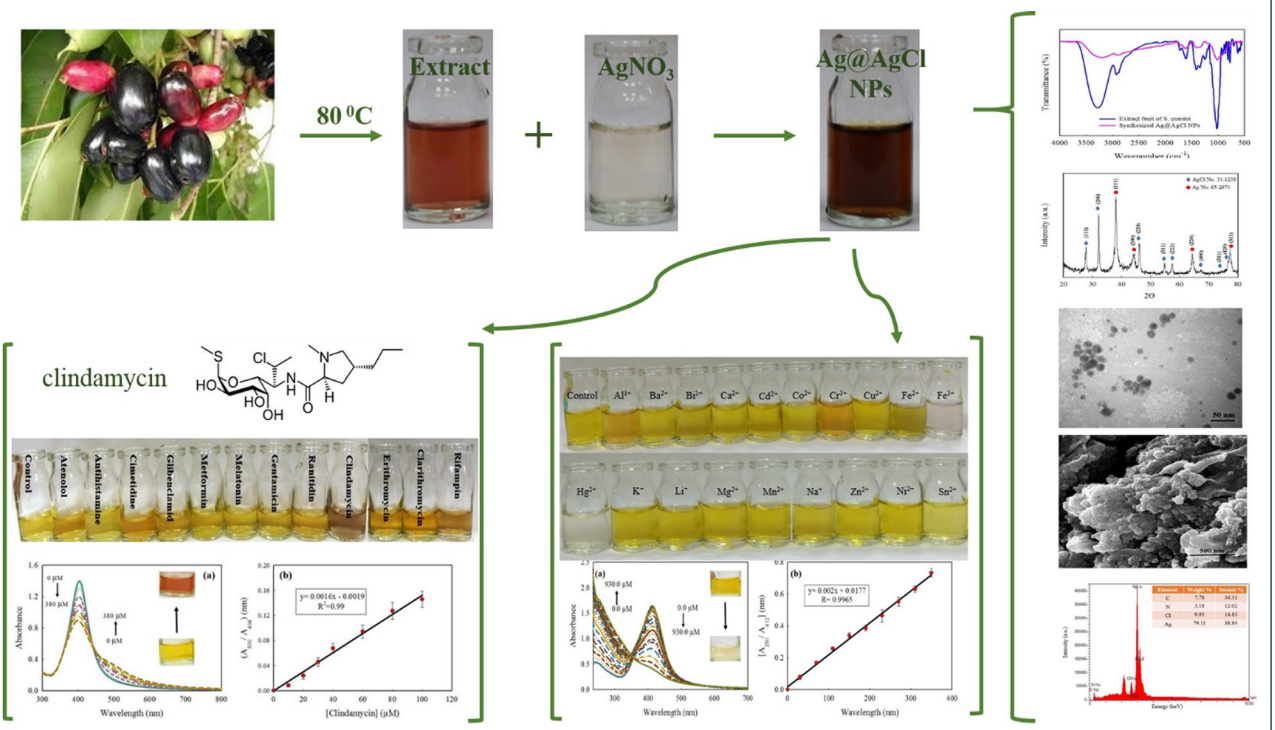

Introduction

With the importance of nanomaterials in all fields of science, their diverse application, and the rapid development of the nanotechnology industry, the research activities of many groups are aimed at synthesizing nanomaterials with specific and desired properties (Ali et al. 2018a, 2018b, 2019a, 2019b, 2021; Khan et al. 2020). Lately, numerous works have been reported for the preparation of metals, metal chlorides, metal sulfides, and metal oxides by the various procedures. Among inorganic nanoparticles (NPs), silver-based nanomaterials, such as silver (Ag), silver chloride (AgCl), and Ag/AgCl nanoparticles have been extensively applied due to their wide physical, chemical, photochemical, biological, biomedical, and antimicrobial properties (Gopinath et al. 2013; Nikaeen et al. 2020; Stalin Dhas et al. 2014; Villanueva-Ibáñez et al. 2015). For these specific properties, Ag-based nanoparticles have gained very application in wastewater treatment, photocatalytic activity and degradation of dyes and organic pollutants, antifungal, antibacterial, antibiofilm, antioxidant, and anticancer agent, and chemical sensing (Devi and Ahmaruzzaman 2016; Feizi et al. 2018; Han et al. 2018; Lombi et al. 2013; Narayanan and Han 2017). Silver-based nanomaterials have been produced by chemical, physical, or biological routes. The physical methods are generally energy-consuming and require sophisticated instruments. The chemical processes involve the utilization of reducer and stabilizer, toxic solvents and chemicals, and generating hazardous waste, that cause restriction of their application in the clinical and biomedical areas. Hence, there is a growing request for cheaper, simpler, cleaner, nontoxic, and ecologically friendly protocols that tend to be available and renewable resources (Eugenio et al. 2016; Gopinath et al. 2013; Kulkarni and Bhanage 2014; Samari et al. 2019; Stalin Dhas et al. 2014). The biological synthesis using various biological systems such as plants, fungi, bacteria, yeasts, actinomycetes, and viruses displays a suitable substitute to physicochemical methods in the synthesis of silver-based nanomaterials. The phyto-synthesis of nanoparticles has a profitable approach and gained significant attention because it is rapid, simple, cost-effective, and easily scaled up to produce well-dispersed nanoparticles with uniform size and shape (Kulkarni and Bhanage 2014; Sharmila et al. 2018; Villanueva-Ibáñez et al. 2015). There have been many reports on the successful production of silver-based nanoparticles, especially Ag NPs, by plant-mediated extracts (Azarudeen et al. 2017; Manivel

and Ilanchelian 2017; Patil Shriniwas 2017; Rajan et al. 2015; Rautela et al. 2019; Samari et al. 2018). In contrast, reports on the phyto-synthesis of Ag/AgCl NPs are less frequent (Devi et al. 2016b, 2016a; Kulkarni and Bhanage 2014). On the other hand, in very fewer cases, the effect of different parameters on the synthesis of Ag/AgCl NPs by plant extracts has been investigated (Al Aboody 2019). Thanks to the existence of various plants and their potency to synthesize nanoparticles, there are several occasions to obtain technologically interesting materials (Villanueva-Ibáñez et al. 2015).

S. cumini is from the Myrtaceae family and is an evergreen tropical tree with possesses hypoglycemic, anti-inflammatory, and antioxidant properties (Bitencourt et al. 2017; Bitencourt et al. 2016). All parts of the *S. cumini* have been widely applied for different medicinal purposes such as antidiabetic, astringent, carminative, stomachic, anti-scorbutic, and diuretic (Mittal et al. 2014). Various phyto-compounds are presented in this plant such as phenols, flavones, tannins, glycosides, amino acids, and alkaloids (Prasad and Swamy 2013). From literature, polyphenols and flavonoids are present in high levels in *S. cumini*. These phyto-molecules are expected to act as reducing agents and cap the formed nanoparticles (Bajpai et al. 2005; Bitencourt et al. 2017; Prasad and Swamy 2013).

Clindamycin (CDM) (Additional file 1: Fig. S1), methyl 6-amino- 7-chloro-6,7,8-trideoxy-N-[(2S,4R)-1-methyl-4-propylprolyl]-1-thio-L-threo-D-galacto octopyranoside-2-(dihydrogen phosphate) is a well-known antibiotic with routine application to treat infections of the respiratory tract, skin, and soft tissue. The bacteriostatic action of clindamycin is primarily against gram-positive aerobes and can be also effective for the anti-infection of a wide range of anaerobic bacteria (Hadi and Honarmand 2017; Ibrahim et al. 2017). On the other hand, a trivalent form of iron (Fe^{3+}) which is the most indispensable and abundant in the natural environment has decisive roles in biological systems, physiological or pathological events (Faizi et al. 2016; Li et al. 2017). Its deficiency or overdose can induce variant disorders (Qin et al. 2008). Additionally, to limit the side effects of drugs based on Fe^{2+} ions, such as gastrointestinal irritation and abdominal pain, the usage of Fe^{3+} complexes has been introduced (Abbaspour et al. 2006). Given the extraordinary importance of clindamycin and Fe^{3+} ions in biological, clinical, and environmental applications, it is really necessary to develop a new and direct determination method for these analytes. Several analytical methods can be found in the literature for the quantitation of clindamycin and iron ions such as electrochemical methods (Hadi and Honarmand 2017; Hu et al. 2016; Wong et al. 2016), spectrofluorimetric method (Faizi et al. 2016; Wahba et al. 2015; Wang et al. 2016), chromatographic methods (Pereira et al. 2018; Schnell et al. 1998), mass spectrometry (Aydin and Soylak 2010; Girondi et al. 2018), and atomic absorption spectroscopy (AAS) (Shamspur et al. 2005). Although each technique has its own merits in one aspect, most of these methods require the use of organic solvents and derivatization of the compound or selective detectors, sophisticated pretreatment, expensive apparatus, elaborate multistep extraction procedures, and trained staff (El-Yazbi and Blaih 1993; Faizi et al. 2016; Li et al. 2017; Vallejos et al. 2016). Therefore, there is still a need for a precise, easy, and convenient alternative method for the measurement of the intended analytes. Moreover, no straight spectrophotometric procedures exist to measure clindamycin. The simplicity and economic advantages of spectrophotometric methods make them highly preferable routes for routine analysis. The lack of an absorbing peak in the UV–Vis region is the main problem in the spectrophotometric determination of clindamycin. In the previous reports, a derivative reaction for the conversion of clindamycin into a UV–Vis active compound was used to measure its concentration spectrophotometrically (Barazandeh Tehrani et al. 2013; El-Yazbi and Blaih 1993), which is not generally an easy and reproducible procedure. So, to quantify the clindamycin in the pharmaceutical dosage form, the development of direct spectrophotometric methods is required (El-Yazbi and Blaih 1993). Considering the abovementioned difficulties, colorimetric sensors rendered an efficient tool for the determination of intended analytes. The colorimetric sensors have some advantages such as ease of construction, simplicity, inexpensive, rapid, and more reliability, and it is possible to have convenient data collection by various cameras or even using the naked eyes (Li et al. 2017).

This study focused on the phyto-synthesis of Ag/AgCl NPs from aqueous fruit extract of *S. cumini*. The effects of different empirical variables on the formation of nanoparticles, such as pH of the solution, concentrations of the silver solution, amount of fruit extract, temperature, and reaction time were studied. To the best of our knowledge, *S. cumini* fruit extract has not been reported for the synthesis of Ag/AgCl NPs despite a recent report on the synthesis of Ag NPs by fruit extracts of *S. cumini* (Mittal et al. 2014). The prepared Ag/AgCl NPs were analyzed by different common characterization tools. Furthermore, phyto-synthesized Ag/AgCl NPs using aqueous *S. cumini* fruit extract were evaluated for their potential as colorimetric sensors toward clindamycin and Fe^{3+} ions.

Materials and methods

Chemicals

Silver(I) nitrate ($AgNO_3$), mercuric(II) chloride ($HgCl_2$), and iron(III) nitrate ($Fe(NO_3)_3$) were purchased from

Merck chemical company, Germany. Clindamycin phosphate was taken from the Sepidaj pharmaceutical company based in Iran. All chemicals used were of reagent grade and were used as received. The solutions of all metal salts (0.1 M) for our runs were prepared from their corresponding metal salts in deionized water. The cleaning of all glassware was intensively attended by rinsing several times with tap water and then re-washed with the deionized water. Deionized Millipore water was used for the reagent preparation. Diluted solutions of hydrochloric acid (HCl) and sodium hydroxide (NaOH) were used to set the pH wherever required.

Preparation of *S. cumini* fruit extract

S. cumini fruits were collected from Bandar Abbas city, Hormozgan province, Iran. The surfaces of freshly collected fruits were cleaned with running tap water, followed by deionized water. Then, the fruit is separated from the core and the prepared fruit samples were dried in shade for 8–10 days, and later, they were finely powdered and stored in a stoppered bottle at the refrigerator at 4 °C for further studies. To prepare fruit extract, 10.0 g of the dried fruit powder and 150 mL of deionized water were mixed in a 250-mL conical flask and then was heated at 80 °C for thirty minutes. After getting cooled, the filtration of the mixture was done through normal filter paper followed by Whatman No. 1 paper. The obtained extract was stored in a refrigerator for further assays and used within a week.

Synthesis of Ag/AgCl NPs

The method includes the simple addition of *S. cumini* fruit extract into the silver(I) nitrate solution at ambient conditions. For typical experiments, a 50-mL Erlenmeyer flask was utilized for mixing 2.0 mL of *S. cumini* fruit extract with 25 mL of 1.0 mM aqueous solution of silver(I) nitrate, and vigorously stirring was applied for 90 min. The reaction development for the production of Ag/AgCl NPs was confirmed from the changing of its color, which was appeared visually from watery yellow to dark brown, and has been followed up quantitatively using UV–Vis spectra.

The various parameters have an effect on the size, shape, dispersity, and optical characteristics of nanoparticles (Singh et al. 2017; Vanaja et al. 2013). Thus, to determine the ideal conditions, the pH of the mixture, the volume of extract, the quantity of metal precursor, temperature of the media, and incubation time were optimized.

The effect of the pH of the mixture solution (3.0, 5.0, 7.0, 9.0, and 11.0), amount of fruit extract (1.0, 2.0, 3.0, 5.0, 7.0, and 10.0 mL), concentration of silver precursor (0.5, 1.0, 2.0, 4.0, and 7.0 mM), the mixture temperature (room temperature (R. T.), 40, 60, and 80 °C), and reaction time on the synthesis of Ag/AgCl NPs were investigated; by keeping constant all parameters except one. The phyto-synthesized NPs were centrifuged at 10,000 rpm for 30 min and rinsed with deionized water. Re-dispersion of the resulting sediments was done in deionized water to rid of any free biological compounds. This procedure was replicated three times to ensure better separation of uncoordinated entities. The dried sediments were used for characterization processes such as Fourier transform infrared (FTIR), X-ray diffraction (XRD), field emission scanning electron microscopy–energy-dispersive X-ray analysis (FESEM–EDS).

Characterization of the synthesized Ag/AgCl NPs

UV–Vis spectra were obtained by SCINCO-S-3100 (Korea) spectrophotometer equipped with a 1.0-cm quartz cell, and all experiments were done at room temperature. The FTIR spectrum was done in the range of 4000–500 cm^{-1} using Bruker alpha (Germany), and an attenuated total reflectance (ATR) cell was utilized for spectral recording. The assessment of the crystal structure of the prepared nanoparticles was performed using a Bruker D8 X-ray diffraction (XRD) (Germany) with Cu-K_{α} radiations. The identification of shape, size, and the elemental study of the prepared Ag/AgCl NPs was performed using sigma-VP (Zeiss, Germany) field emission scanning electron microscopy–energy-dispersive X-ray analysis (FESEM–EDS). Transmission electron microscopy (TEM) studies were carried out by Zeiss–EM10C with an accelerating voltage of 80 kV.

Colorimetric sensing of clindamycin using Ag/AgCl NPs

The Ag/AgCl NPs-based colorimetric method was used to measure clindamycin. The pH of the sensing solution and reaction time were optimized. To optimize the pH of the reaction mixture, the sensing process was run at different pH (3.0–11.0 with an interval of 2). That way, 35.0 µL of 0.01 M of clindamycin solution was injected into 2.5 mL of diluted solution of Ag/AgCl NPs (with ratio 1:4) with adjusted pH, and the alteration in the color of the obtained mixture was followed using UV–Vis absorption spectra. At the optimized pH, the absorbance of the reaction mixture was measured at different time intervals. In following, at the optimized reaction conditions, the calibration curve was obtained by consecutive injecting of different µL volumes of clindamycin into 2.5 mL of the diluted Ag/AgCl NPs.

To investigate the selectivity of the proposed sensor for clindamycin, different drugs (atenolol, antihistamine, cimetidine, glibenclamide, metformin, melatonin, gentamicin, ranitidine, erythromycin, clarithromycin, rifampin) were checked. Some of these drugs have similar

use/activity, and some others have been patented because of their broad spectrum of activity (Paul et al. 2017; Pereira et al. 2018). Because of the popularity of clindamycin and some other list of antibiotics, there are falsified and fake copies of the antibiotics on the market (Paul et al. 2017) and the exact determination of clindamycin is important. Some of these selected drugs such as rifampin also are currently used in combination with clindamycin to treat severe infectious diseases in hair follicles (Pereira et al. 2018; van der Zee et al. 2009). On the other hand, some of the selected compounds were studied as interference to show the potential of determination of clindamycin in wastewater or complex biological samples for future works. Each of these drugs (50.0 μM) was added separately into 2.5 mL of diluted Ag/AgCl NPs solution at the optimized pH, and the sample vials were kept for a few minutes at room temperature. The changes of color were monitored via a digital camera and the UV–Vis absorption spectrometer.

Finally, the proposed colorimetric sensor was applied for determinations of clindamycin in pharmaceutical formulations. Two commercial pharmaceutical formulations of clindamycin (clindamycin capsules from Daroupakhsh distribution company, Iran, contain 150 mg clindamycin hydrochloride per capsule based on its commercial label, and clindamycin injection dosage, 150 mg mL^{-1}, from Tehran Chemie Daroo, Iran) were purchased from local drugstores and used as real samples. Ten capsules were finely grounded and well mixed. The equivalent of one capsule was accurately weighed, dissolved in deionized water, and then filtered by 0.45-μm pore size Biofilm filters, to separate insoluble materials. After the transfer of the solution to a 10-mL volumetric flask, the final volume was adjusted to the mark with deionized water. The concentration of clindamycin was 0.035 M in this prepared solution. 8.6 μL of the above-prepared clindamycin capsule solution was added into 2.0 mL of the freshly synthesized Ag/AgCl NPs solution in 10-mL volumetric flasks, and the volume was adjusted with deionized water and mixed well. Determination of clindamycin was done via the standard addition approach. For injection dosage form of clindamycin, 0.86 μL of the ampoules, labeled to contain 150 mg mL^{-1} (equivalent to 0.35 M) of clindamycin phosphate per ampoule, was added into 2.0 mL of the freshly synthesized Ag/AgCl NPs in 10-mL volumetric flasks and the next steps were the same approaches as previously mentioned.

Detection ability of the synthesized Ag/AgCl NPs for Fe^{3+} ions

The detection capability of the as-synthesized Ag/AgCl NPs to metal ions was checked. For this goal, different metallic salts ions (Li^+, Na^+, K^+, Ba^{2+}, Ca^{2+}, Mg^{2+}, Al^{3+}, Bi^{3+}, Cd^{2+}, Co^{2+}, Cu^{2+}, Fe^{2+}, Fe^{3+}, Hg^{2+}, Mn^{2+}, Ni^{2+}, Sn^{2+}, and Zn^{2+}) at the same conditions (10.0 μL, 10^{-1} M) were added into the diluted solution (with ratio 1:4) of Ag/AgCl NPs (2.5 mL). UV–Vis absorption spectra were utilized to follow the alteration in the color of the examined solutions. After surveying the UV–Vis absorption spectra and color change of the assay solutions after the addition of different metal ions, the Fe^{3+} ion was selected for further sensing. In the following, the influence of the reaction mixture pH and time was optimized to get the highest sensitivity in the determination of Fe^{3+} ions.

In the following, the spectrometric detection of Fe^{3+} ion was carried out by adding different volumes (in microliter) of a solution of 0.001 M Fe^{3+} into the 2.5 mL of the diluted solution of Ag/AgCl NPs (adjusted to optimized pH). The absorption spectra of the mixture were monitored via a UV–Vis spectrophotometer.

The applicability of the suggested approach for the determination of Fe^{3+} in the real medium was checked using two water samples: tap water (Molecular Medicine Research Center, Hormozgan Health Institute, Hormozgan University of Medical Sciences, Bandar Abbas, Iran) and mineral water (MALAS Company, Iran). The concentration of Fe^{3+} in the studied real samples was initially checked by atomic absorption spectrometry (240 FS, Agilent Technologies, USA). In this work, 1.0 mL of each kind of water was tested in a 10-mL volumetric flask, mixed with 2.0 mL of the synthesized Ag/AgCl NPs, adjusted to the mark with deionized water, and mixed well. The standard addition method was used for quantitation of Fe^{3+} ions in such a way that into 2.0 mL of the above solution (adjusted to optimized pH) various volume of a standard solution of Fe^{3+} was added, and the absorbance of the obtained mixture was collected 1 min after each addition.

Results and discussion

Visual observations and UV–Vis spectral studies

The addition of the aqueous fruit extract of *S. cumini* to the prepared silver ions solution causes a color alternation in the mixture, and it changed from light yellow to brown. This color change of the mixture solution qualitatively confirmed the production of Ag/AgCl NPs and can be spectrally followed by the surface plasmon resonance (SPR) of the formed nanoparticles (Mulvaney 1996; Tripathy et al. 2010). Furthermore, an intense and sharp SPR peak at around 412 nm confirmed the formation of Ag/AgCl NPs as shown in Fig. 1. Although numerous methods are reported in the literature for Ag/AgCl NPs synthesis, most of them used toxic materials (Song et al. 2013; Wang et al. 2008). The use of green and clean technology is expected to minimize pollution in the environment. In this work, *S. cumini*

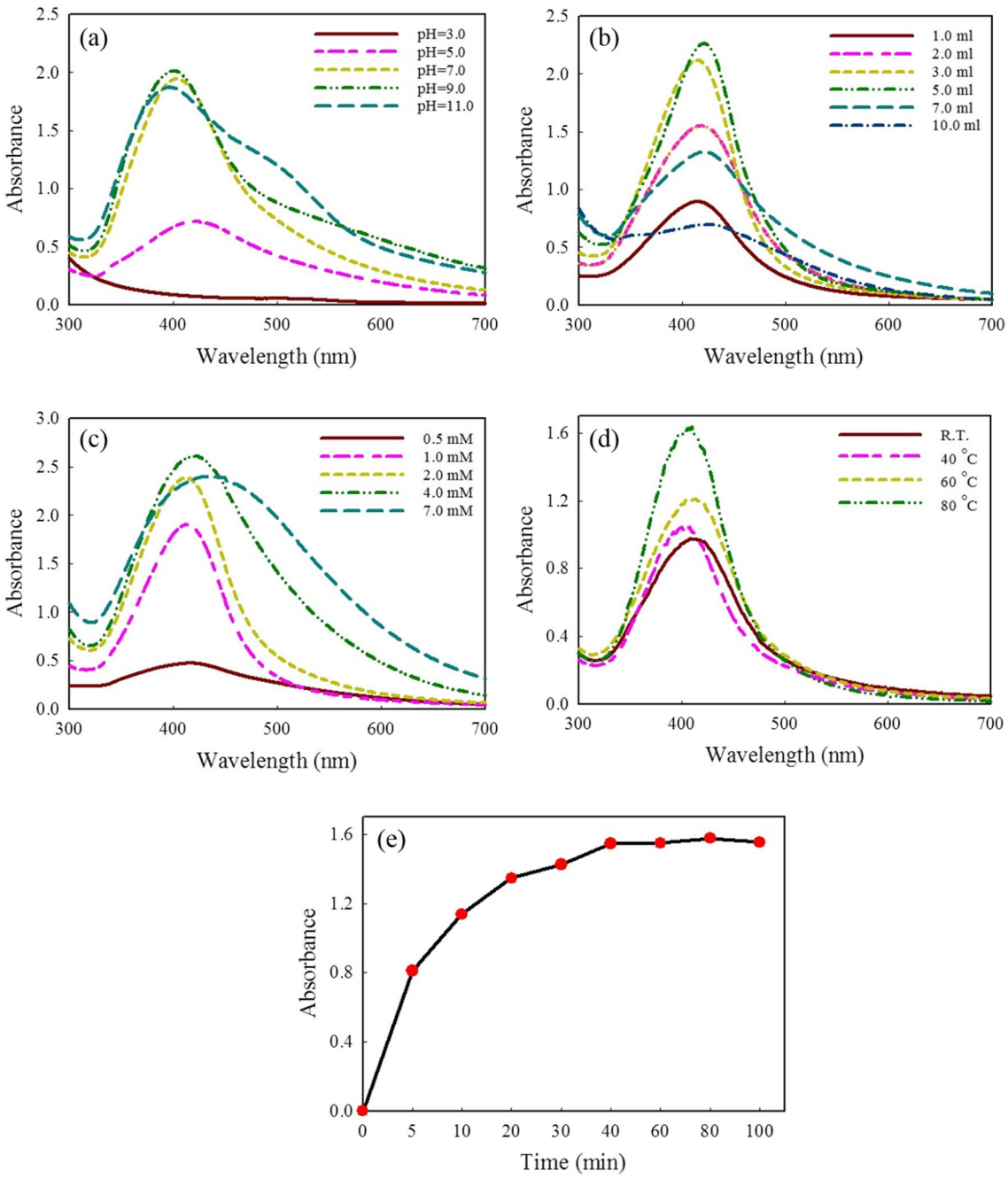

Fig. 1 UV–Vis absorption spectra of the Ag/AgCl NPs synthesized at **a** different pH from 3 to 11, **b** different *S. cumini* fruit extract content from 1 to 10 mL, **c** different silver nitrate concentration from 0.5 to 7.0 mM, **d** different reaction temperature (R. T. , 40, 60, and 80 °C), and **e** optimization of the reaction time

fruit extract was adopted for the green fabrication of Ag/AgCl NPs because it is inexpensive and environmentally friendly. The available phytochemicals in the *S. cumini* fruit extract can serve multiple functions as reducing and stabilizing agents and halide sources in the synthesis of Ag/AgCl NPs. The proposed method is a novel approach that avoids the use of any external reducing and capping agents, toxic solvents, and external halide ion sources.

Optimization of the phyto-synthesis of nanoparticles

To study the effect of pH on the production of NPs, the synthesis procedure was run at different pH (3.0, 5.0, 7.0, 9.0, and 11.0), while, the other parameters like the quantity of silver precursor (25 mL, 1.0 mM), the volume of *S. cumini* fruit extract (2.0 mL), reaction temperature (R. T.), and incubation time (1.5 h) were kept constant. The UV–Vis spectra of the mixture at different pH were monitored during the production of Ag/AgCl NPs and are shown in Fig. 1a. Our results show that the pH of the reaction has a main effect on the construction of Ag/AgCl NPs. At pH of 3.0, no characteristic peak of Ag/AgCl NPs was observed, due to suppression of the nanoparticle production in acidic media (Vanaja et al. 2013). As the pH of the reaction media increased from 3.0 to 7.0, the SPR intensity of the formed nanoparticles gradually increased accompanied by the blueshift from 407 to 404 nm. At pH 9.0, the absorbance intensity was near to its value at pH 7.0, although the SPR band became wider and the λ_{max} is shifted to 400 nm which indicates smaller particles synthesis with a wider size distribution. These observations suggest the formation of smaller particles with higher formation rates in media with basic and neutral pH that is due to the ionization of phenolic compounds in the utilized extract (Samari et al. 2018). The low production rate of nanoparticles in acidic media is due to the lower activity of phyto-molecules reducer and the aggregation of synthesized nanoparticles to form larger particles (Saware and Venkataraman 2014). At pH 11.0, the absorbance intensity was decreased and the peak broadening was observed. Also, agglomeration or precipitation was seen after 24 h at higher pHs (9.0 and 11.0) because of the lower stability of the synthesized nanoparticles or the absence of a stabilizer (Vanaja et al. 2013). It was found that a neutral medium (pH of 7.0) produced more stable nanoparticles with a smaller size distribution. Therefore, pH 7.0 was considered as an optimum pH for further study.

In Fig. 1b, the absorption spectra of the synthesized nanoparticles by adding the various quantities of fruit extract (1.0, 2.0, 3.0, 5.0, 7.0, and 10.0 mL) to 25 mL of 1.0 mM of $AgNO_3$ were shown (the temperature, incubation time, and pH were R. T., 1.5 h, and 7.0, respectively). The resulting spectra have shown a great dependency of the formed nanoparticles on the quantity of fruit extract that acts as a capping and reducing agent. By increasing the quantity of extract from 1.0 to 5.0 mL, the SPR intensity was increased, mainly due to the construction of more nanoparticles. Also, the λ_{max} of the SPR band shifted to a longer wavelength, which confirms the formation of larger particles. In fact, by increasing the volume of fruit extract, excess amounts of reducing agents in the extract could be bound to the preformed nuclei's surface and cause the additional reduction of metal ions. Subsequently, the increase in the growth rate of nanoparticles happened and larger particles are formed (Tahir et al. 2015; Yang and Li 2013). Having a further increase in the extract volume (7.0 and 10.0 mL), a decrease in the absorbance accompanied by band broadening was observed, as presented in Fig. 1b, which indicates a larger size distribution of the formed nanoparticles. Concerning the stability of the synthesized nanoparticles, the application of a 3.0 mL fruit extract solution for reacting to $AgNO_3$ solution causes more stability than others. It was reported that a high quantity of reducing agents can enhance the bridging effect between the formed nanoparticles and lead to the aggregation of nanoparticles (Yang and Li 2013). From the above discussion, the optimized quantity of *S. cumini* fruit extract for the preparation of Ag/AgCl NPs in the presence of 25 mL of $AgNO_3$ (1.0 mM) was selected to be 3.0 mL.

The effect of concentration of $AgNO_3$ solution during the preparation of nanoparticles was examined by exposing 3.0 mL of fruit extract of *S. cumini* to 25 mL of $AgNO_3$ with different concentrations (0.5, 1.0, 2.0, 4.0 and 7.0 mM) at pH 7.0 and room temperature for 1.5 h. The UV–Vis spectra of the resultant Ag/AgCl NPs colloidal solution by different concentrations of the silver salt solution are shown in Fig. 1c. By enhancing the concentration of silver precursors from 0.5 to 4.0 mM, the SPR intensity was enhanced due to an increase in nanoparticles formation. Thereafter, at 7.0 mM, the absorbance intensity started to decrease because the applied quantity of fruit extract might not be enough to reduce all existing silver ions, and hence peak intensity was decreased. Also, with an increase in the silver ion concentration, the SPR band shifted to red (from 412 to 421 nm) and band broadening occurred, which represents the synthesis of larger particles with a wider size distribution. The reason for this observation is an enhancement in agglomeration after the addition of more metal ion amounts (Saware and Venkataraman 2014). It is necessary to mention that similar results have been obtained in other researches (Vanaja et al. 2013; Yang and Li 2013). Therefore, 1.0 mM of $AgNO_3$ solution is more appropriate to get a high concentration of nanoparticles with a smaller size, more stable, and narrower size distribution.

To study the effect of reaction temperature on the synthesis of nanoparticles, the reaction was done at four different temperatures (room temperature, 40, 60, and 80 °C), keeping the volume of fruit extract constant at 3.0 mL, 25 mL of 1.0 mM of $AgNO_3$, pH of 7.0, and 1.5 h. The resulting absorbance spectra of the synthesized nanoparticles at four temperatures are shown in Fig. 1d. Based on the obtained data, it could be concluded that the reduction process is related to the

reaction temperature and a higher temperature leads to more production of nanoparticles. It is worthy to note that in higher temperature (>80 °C) such as 90 °C, no enhancement was observed SPR peak. On the other hand, the SPR in high temperature (80 °C and higher) was not repeatable but repeatability was better in 60°. However, a more intense SPR peak was obtained at 80 °C, for energy saving and more difficulty in the adjustment and to obtain repeatable SPR, the temperature of 60 °C was utilized as the optimum.

The kinetics of the synthesis procedure was performed by following the reduction process and recording the absorbance value at different time intervals. Figure 1e shows the SPR intensity at 412 nm from the reaction between aqueous silver nitrate and fruit extract (at the optimum condition) as a function of time. It was found that the production of nanoparticles is started almost immediately after the addition of the fruit extract, and this continued throughout the investigation process (as shown by the progressive enhancement in the absorbance intensity at 412 nm) and remained unchanged after 40 min of incubation, that is confirmed the reaction process is completed at 40 min. Thus, it is obvious that the *S. cumini* fruit extract has a potent capability to make and stabilize nanoparticles and the reduction was done faster than some of the reports about the plant-mediated synthesis of Ag/AgCl NPs (Chen et al. 2000; Chyau et al. 2006; Kinoshita et al. 2007).

Characterization of nanoparticles

X-ray diffraction (XRD) studies

The crystalline structure of the Ag/AgCl nanoparticles was identified using XRD study, and the obtained pattern is shown in Fig. 2a. The peaks at 2θ values of 27.8°, 32.2°, 46.2°, 54.9°, 57.6°, 67.4°, 74.9° and 76.7° have belonged to the (111), (200), (220), (311), (222), (400), (311), and (420) lattice planes of the cubic silver chloride NPs, respectively (ICDD file no. 31-1238) (da Silva Ferreira et al. 2017; Zhao et al. 2015). The remaining peaks at 38.2°, 44.6°, 64.4° and 77.2° were indexed of the formation of (111), (200), (220), and (311) planes in the face-centered cubic (FCC) structure of silver, respectively (JCPDS file: 65-2871) (Devi et al. 2016b). It is noteworthy that found no other characteristic peaks in the obtained XRD spectra, which confirmed the high crystal phase purity of the formed Ag/AgCl NPs.

TEM, FESEM, and EDS studies of S. cumini synthesized Ag/AgCl NPs

The TEM study was conducted to investigate the size, morphological features, and dispersion of the produced Ag/AgCl NPs, and the corresponding image is shown in Fig. 2b. TEM images revealed that the formed Ag/AgCl NPs were almost spherical with an average size of 16.9 nm. Also, the image displays that the synthesized Ag/AgCl NPs are well dispersed without significant agglomeration.

Further, FESEM images of the prepared nanoparticles confirmed the formation of spherical particles with a size between 20 and 24 nm (Fig. 2c), which matches the TEM images. The elemental analysis of the prepared Ag/AgCl NPs was done by using EDS measurement, as shown in Fig. 2d. The obtained results that show two peaks with high intensity were corresponding to Ag and Cl, which indicate the presence of Ag/AgCl. Thus, fruit extract acts as the chloride ion supplying agent as well as reducer and capping agents that are naturally available for the formation of Ag/AgCl NPs.

FTIR measurement

FTIR spectra were used to clarify the possible functional groups of phyto-compounds presented in the surface of the synthesized Ag/AgCl NPs that may be responsible for the reduction of Ag^+ ions and stabilization of the formed Ag/AgCl NPs. The obtained FTIR spectra of *S. cumini* fruit extract and synthesized Ag/AgCl NPs are presented in Fig. 2e. The FTIR spectrum of *S. cumini* fruit extract indicates a broad and intense absorption peak at 3277 cm^{-1} related to stretching vibrations of the hydrogen-bonded O–H in alcohols and phenolic compounds such as flavonoids or amines (N–H group) (Devi et al. 2016b). The peaks at 2931 cm^{-1} and 2890 cm^{-1} were attributed to C–H stretching symmetric and antisymmetric modes of aliphatic and aromatic compounds, respectively (Gong et al. 2018). The presence of an intense absorption band in the range between 1750 and 1520 cm^{-1} could be attributed to C=C, carbonyl (C=O), or –N–H stretching vibrations of amide I and amide II, which is perhaps due to the presence of proteins/peptides that could act as stabilizing agents as well as reducing agents in the formation of Ag/AgCl NPs (Gong et al. 2018). The peaks at 1266 cm^{-1} and 1023 cm^{-1} can be indicators of the C–O and C=O of aromatic acids and esters, respectively (Durán et al. 2014).

The FTIR spectrum of the synthesized Ag/AgCl NPs demonstrates distinct peaks at 3202, 2918, 2878, 1621, 1407 and 1013 cm^{-1} (Fig. 2e). The comparison of the obtained spectra of the *S. cumini* fruit extract and the as-prepared Ag/AgCl NPs showed slight shifts in the peak positions as well as a decrease in the intensities. In particular, the shift of peak from 3277 to 3202 cm^{-1} may also indicate the involvement of the O–H functional group in the reduction of Ag^+ ions and formation of Ag/AgCl NPs (Devi et al. 2016a). Also, the shift of peaks 2931 and 2890 cm^{-1} to 2918,

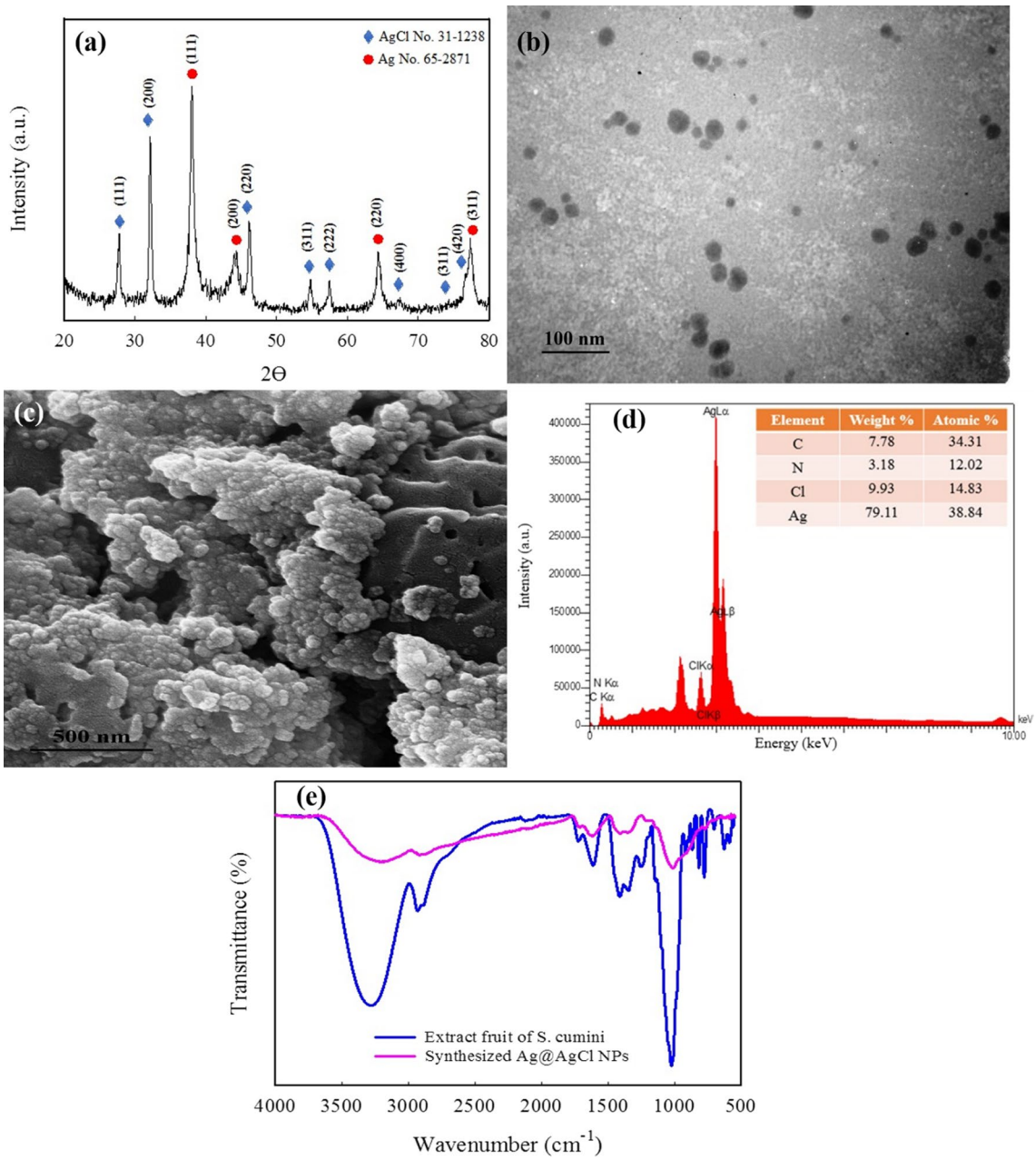

Fig. 2 **a** XRD pattern, **b** TEM image, **c** FESEM image, **d** EDS pattern, and **e** FTIR spectrum for Ag/AgCl NPs synthesized by aqueous fruit extract of *S. cumini*

2878 cm^{-1}, respectively, in the synthesized NPs indicates the involvement of bonds C–H of aliphatic and aromatic compounds in NPs synthesis (Patil et al. 2017). On the other hand, the appeared bands of fruit extract in the FTIR spectrum of the synthesized NPs revealed that phyto-constituents also protected the as-prepared Ag/AgCl NPs from aggregation (Devi et al. 2016a). From these results, it can be concluded that phyto-compounds in the *S. cumini* fruit extract drive the bio-reduction of Ag^{+} ions into silver nanoparticles (Ag^{0}) and facilitate the formation and stabilization of Ag/AgCl NPs (Devi et al. 2016a; Gopinath et al. 2013; da Silva Ferreira et al. 2017). However, further studies are needed to confirm our results and to understand the exact role of *S. cumini*-derived bio-compounds in Ag/AgCl NPs production.

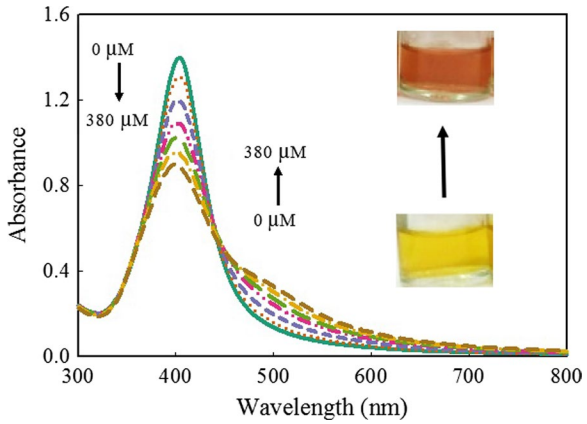

Fig. 3 UV–Vis spectrum of diluted nanoparticles in the presence of different amounts of clindamycin and related color change as inset

Sensing ability of the synthesized Ag/AgCl NPs toward clindamycin

The colorimetric sensing of an intended analyte is one of the most interesting methods because UV–Vis spectrophotometer is widely available and provides the naked-eye sensing of the analyte (Tavallali et al. 2013). By adding clindamycin to the diluted solution of the synthesized nanoparticles, the yellow color of the nanoparticles solution is changed to pink. From absorption studies, the SPR band of the synthesized Ag/AgCl NPs was shifted to red. This could be owing to the aggregation of nanoparticles in the presence of clindamycin and the decrease in the distance between nanoparticles. To achieve the maximum sensitivity of the proposed sensor to clindamycin, the pH of the solution, in the wide range of 3.0–11.0, and incubation time (in the presence of 14.0×10^{-5} M of clindamycin) were optimized and the obtained results are presented in Additional file 1: Fig. S2. The magnitude of the absorbance ratio of A_{500}/A_{404} was used as a signal for clindamycin detection. According to Additional file 1: Fig. S2a, the pH of 3.0 showed better sensitivity and was selected in the following experiments. Moreover, Additional file 1: Fig. S2b shows the increase in the magnitude of A_{500}/A_{404} from 1 to 3 min and after that became approximately constant. Therefore, the measurement was carried out 3 min after each injection.

Quantitative analysis was carried out by the injection of different concentrations of clindamycin into synthesized Ag/AgCl NPs solution, and the UV–Vis absorption spectra and color changes were recorded after 3 min of the addition of the drug. Figure 3 represents the SPR band of the synthesized Ag/AgCl NPs and its typical change during the addition of the different concentrations of clindamycin. The more increases in the concentration of the clindamycin resulted in more decrease in the absorbance at 404 nm accompanied by an increase in the absorbance at 500 nm. The linear range of the proposed method obtained from the relationship between A_{500}/A_{404} ($y = 0.0016x - 0.0019$) and the concentration of clindamycin is shown in Additional file 1: Fig. S3. Good correlation coefficients ($R^2 = 0.99$) and low detection limit (1.23 µM) with an acceptable linear dynamic range (over the range of 10.0–100.0 µM) are the main characteristics of the suggested method. These results represented the high efficiency of the synthesized Ag/AgCl NPs in the detection of clindamycin.

To evaluate the selectivity of the synthesized Ag/AgCl NPs toward clindamycin, uniform concentrations (35.0 µM) of several drugs (atenolol, antihistamine, cimetidine, glibenclamide, metformin, melatonin, gentamicin, ranitidine, erythromycin, clarithromycin, and rifampin) were added into the diluted solution of the synthesized nanoparticles. After a few minutes, the change in the color of the Ag/AgCl NPs solution was seen from yellow to pink only in the presence of clindamycin, and other drugs did not have any obvious color change. In Additional file 1: Fig. S4a and b, spectral changes and photograph images of the Ag/AgCl nanoparticles solution with different drugs were displayed, respectively. These results confirm that other tested drugs had little or no obvious effect on the color change and absorption spectra. Therefore, the proposed sensor has high selectivity toward clindamycin.

To survey the real sensing ability of the synthesized Ag/AgCl NPs in the detection of clindamycin, the sensing efficiency in pharmaceutical preparations (capsule and injection dosage) was done. The recovery of the proposed method was determined by spiking the clindamycin in two different real samples with known amounts of clindamycin, and the obtained results are presented in Table 1. The mean recovery values for clindamycin in the pharmaceutical samples were found to be 92.6–104.9% with relative standard deviation (RSD) values < 7%. Our study demonstrates that the proposed sensor could be acceptably applied in the quality control of clindamycin in the capsule and injection dosage forms.

In Table 2, the efficiency of our method is compared with several existing analytical methods for the determination of clindamycin in different matrices. Although the limit of detection (LOD) of most of the previous methods (Dedić et al. 2018; Habib et al. 2011; Kowalski et al. 2014; Liang et al. 2014; Liu et al. 2010; Pereira et al. 2018; Shao et al. 2006; Stanković et al. 2013; Szultka-Mlynska et al. 2018) is better than our method, most of these procedures have one or more disadvantages such as being laborious, time consuming, nonspecific, less safe, and too expensive. Our proposed method has the advantage of the high simplicity of optical sensors procedures

Table 1 The amounts of spiked clindamycin into the capsule and vial of clindamycin samples

Sample	Spiked (μM)	Expected (μM)	Found (μM)	Recovery (%)	RSD (%)
Clindamycin capsule	0	30	31.4	104.9	6.4
	10	40	39.6	99.1	5.9
	20	50	49.0	98.1	6.7
	40	70	68.0	97.1	5.8
	70	100	101.0	101.0	6.2
Clindamycin vial	0	30	30.9	103.0	6.1
	10	40	38.4	96.0	3.8
	20	50	46.3	92.6	2.8
	40	70	65.0	92.9	3.8
	70	100	101.4	101.4	3.9

Table 2 Dynamic range and LOD of the presented Ag/AgCl NPs sensor for determination of clindamycin and its comparison with other methods

Sample	Method	Dynamic rang (μM)	LOD (μM)	References
Clindamycin	Chemiluminescence	2.3×10^{-4}–0.2	7.1×10^{-5}	Shao et al. (2006)
Clindamycin hydrochloride	UV–Vis	$(1.2–5.9) \times 10^{2}$	1.8×10^{-6}	Dedić et al. (2018)
Clindamycin phosphate	HPLC	23.5–188.2	23.4	Stanković et al. (2013)
Clindamycin phosphate	UV–Vis-HPLC	1.2–47.1	0.3	Pereira et al. (2018)
Clindamycin phosphate	NMR	$(1.7–5.4) \times 10^{4}$	94.1	Liang et al. (2014)
Clindamycin	HPLC–MS	2.4–117.6	0.1	Szultka-Mlynska et al. (2018)
Clindamycin	Electrochemiluminescence	0.5–100.0	1.3×10^{-2}	Liu et al. (2010)
Clindamycin	Voltammetry-DP	0.2–1.0	0.1	Habib et al. (2011)
Clindamycin	Voltammetry-SW	0.2–1.9	0.2	Habib et al. (2011)
Clindamycin	Ag/AgCl NPs	10.0–100.0	1.2	This work

without the need to perform any derivative reaction to convert the clindamycin into UV–Vis absorptive species. Furthermore, the synthesis of Ag/AgCl NPs is direct, one step, simple, economical, and eco-friendly without the addition of any hazardous reagents. Finally, with our proposed method, the determination of clindamycin in each sample is relatively fast.

Sensing ability of the synthesized Ag/AgCl NPs toward Fe^{3+}

The colorimetric sensing ability of the Ag/AgCl NPs towards various metal ions such as Li^{+}, Na^{+}, K^{+}, Ba^{2+}, Ca^{2+}, Mg^{2+}, Al^{3+}, Bi^{3+}, Cd^{2+}, Co^{2+}, Cu^{2+}, Fe^{2+}, Fe^{3+}, Hg^{2+}, Mn^{2+}, Ni^{2+}, Sn^{2+}, and Zn^{2+}, under the identical conditions, was explored in aqueous solution. In Additional file 1: Fig. S5a and b, the absorption band of the diluted Ag/AgCl NPs solution and its photographic images during adding of various metal ions are presented, respectively. Additional file 1: Fig. S5a displays that with the addition of diverse metal ions into the Ag/AgCl NPs solution, only Fe^{3+} and Hg^{2+} can result in discoloration. Owing to this considerable decrease in the SPR intensity, the facility of developing a sensitive procedure for the measurement of Fe^{3+} ions based on UV–Vis absorption spectroscopy has been investigated. The addition of other metal ions to the colloidal solution of Ag/AgCl did not depict a remarkable change in the color, demonstrating no significant interferences from other metal ions in the detection of Fe^{3+} ions. Although Hg^{2+} ions could also cause a significant decrease in the absorption intensity, according to previously reported studies (Basiri et al. 2018; Gao et al. 2015), this challenge could be circumvented by the addition of L-cysteine to the sensing solution as a masking agent of Hg^{2+}. It is because of this fact that the Hg^{2+} has a major attitude to L-cysteine and could display a large sheltering effect to Fe^{3+} ions. Therefore, the selectivity of the proposed sensor toward Fe^{3+} probably could be improved.

In the following, the Ag/AgCl NPs assay for analytical detection of Fe^{3+} was optimized. The effect of the pH of the sensing solution and reaction time was studied. The pH condition in the detection of Fe^{3+} ions, using a colloidal solution of Ag/AgCl NPs in the presence of 4.0×10^{-6} M Fe^{3+} ions, was optimized in the wide

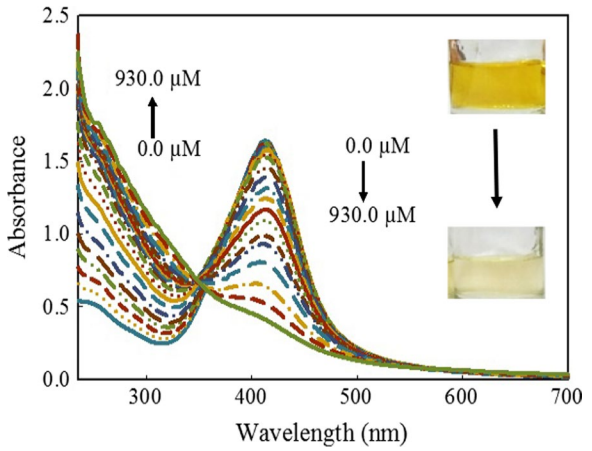

Fig. 4 UV–Vis absorption spectra of diluted nanoparticles solution in the presence of different amounts of Fe^{3+} ion and related color change as inset

range of 3.0–11.0, and the obtained results are displayed in Additional file 1: Fig. S6a. The change in the absorbance intensity, ΔA ($\Delta A = A_0 - A_t$, where A_0 and A_t are the absorbance intensity of the Ag/AgCl NPs solution at 412 nm before and after the addition of Fe^{3+} ions, respectively), was applied as the analytical signal in the determination of Fe^{3+}. Corresponding to Additional file 1: Fig. S6a, pH 9.0 was selected as an appropriate pH in the detection of Fe^{3+} ions. At pH of 9.0, more change in the color and spectral of Ag/AgCl NPs was noted. Also, Additional file 1: Fig. S6b represents the ΔA values from 1 to 5 min after the addition of Fe^{3+} ions. From Additional file 1: Fig. S6b, ΔA value became almost constant 1 min after the addition of Fe^{3+} ions, Therefore, the reaction was monitored 1 min after each addition of Fe^{3+} ions.

To calculate the linear dynamic range of concentration of Fe^{3+} ions in an aqueous solution, under the optimized conditions, the various concentrations of Fe^{3+} ions (10.0–930.0 µM) were added to Ag/AgCl NPs solution. From Fig. 4, as the concentration of Fe^{3+} ions increased, the SPR intensity gradually decreased, accompanied by a slight blueshift, and the sensing solution color changed from yellow to colorless (Fig. 4 inset). The blueshift suggests the reduction in the size of Ag/AgCl NPs in the presence of Fe^{3+} ions. In fact, with the addition of Fe^{3+} ions to the Ag/AgCl NPs solution, the Ag/AgCl NPs can be decomposed by Fe^{3+} ions, and its result is a gradual decrease in the SPR intensity dependent on Fe^{3+} concentration (Gao et al. 2015). The obtained linear range was 10.0–350.0 µM of Fe^{3+} ($y = 0.002x - 0.0177$, $R^2 = 0.9965$) with LOD of 1.2 µM (S/N = 3, $n = 3$) (Additional file 1: Fig. S7). In Table 3, the comparison between different sensing systems for the determination of Fe^{3+} ions is summarized. The proposed sensing probe displayed an appropriate LOD and linear range as well as speciation toward Fe^{3+} ions without the interference effect of Fe^{2+} ions, compared with the other methods. On the other hand, the semiquantitative measurement of Fe^{3+} ions could be attained by naked eyes when the solution color changed.

To investigate the feasibility of the proposed sensing method, the standard addition procedure was applied to detect Fe^{3+} ions in water samples. First, the concentration of Fe^{3+} was determined in the investigated water samples (mineral and tap water) using atomic absorption with Flame atomization. Different concentrations of Fe^{3+} ions standard solution were added into mineral and tap water samples. After adding the desired real water to the designed sensing system, no change was observed in the yellow color of the mixture solution with no significant difference between the utilized blank solution and the added water samples in the UV–Vis absorbance. Hence, it was assumed that the Fe^{3+} ions concentration of water samples is zero or undetectable. The obtained results by the proposed method are shown in Table 4. Mean recovery values for Fe^{3+} ions in the spiked samples showed the accuracy of the proposed sample which was in the range of 90.5–109.5% and the RSD values lower than 6% confirmed its precision. According to the results, the suggested approach can be a low-cost way and portable platform for sensing Fe^{3+} ions in environmental water based on bioengineered Ag/AgCl NPs with great potential in selectivity and accuracy.

Table 3 Dynamic range and LOD of the presented Ag/AgCl NPs sensor for determination of Fe^{3+} and its comparison with other nanoparticles-based colorimetric methods

Nanostructure	Dynamic range (µM)	LOD (µM)	References
Au NPs	17.9–89.5 ($\times 10^{-4}$)	89.5×10^{-5}	Tripathy et al. (2013)
Modified Au NPs	10–60 ($\times 10^{-6}$)	5.6×10^{-6}	Wu et al. (2011)
Modified Au NPs	10–100 ($\times 10^{-9}$)	9.4×10^{-9}	Pandya et al. (2013)
Modified Au NPs	40–80 ($\times 10^{-6}$)	1.5×10^{-8}	Mehta et al. (2014)
Modified graphene oxide quantum dot	10^{-7}–10^{-3}	1×10^{-7}	Baruah and Chowdhury (2016)
Ag/AgCl NPs	0–350 ($\times 10^{-6}$)	1.24×10^{-6}	This work

Table 4 Fe^{3+} ion recovery rates added in tap and mineral water samples

Sample	Spiked (μM)	Found (mean ± SD, μM) with our method	Found (mean ± SD, μM) with AAS	Recovery (%)	RSD (%)
Mineral water	0	8.44 ± 0.01	8.38 ± 0.03	100.7	5.09
	52.8	53.22 ± 0.01	Not checked	100.8	2.90
	105.6	95.60 ± 0.01	Not checked	90.5	2.92
	158.4	149.71 ± 0.02	Not checked	94.5	4.67
	211.2	213.91 ± 0.03	Not checked	101.2	5.27
	264	252.50 ± 0.03	Not checked	95.6	4.34
	316.8	311.21 ± 0.04	Not checked	98.2	5.42
Tap water	0	10.66 ± 0.01	10.75 ± 0.02	99.16	1.85
	52.8	57.84 ± 0.03	Not checked	109.5	3.02
	105.6	98.60 ± 0.02	Not checked	93.3	2.81
	158.4	148.88 ± 0.03	Not checked	93.9	3.77
	211.2	194.99 ± 0.04	Not checked	92.3	4.17
	264	261.89 ± 0.02	Not checked	99.2	2.33
	316.8	381.75 ± 0.02	Not checked	101.6	2.80

Conclusion

Ag/AgCl NPs were synthesized via a one-step, simple, eco-friendly, and economical route by fruit extract of *S. cumini* without taking recourse to any surfactant and halide source. The effect of various parameters on the production of Ag/AgCl NPs was optimized. The optimal conditions were determined to be: pH = 7.0, the quantity of the leaf extract = 3.0 mL, 25 mL silver precursor with the concentration of 1.0 mM, temperature = 60 °C, and incubation time = 40 min. The synthesis of Ag/AgCl NPs was endorsed by monitoring the color change of the reaction media and showing the SPR at 412 nm. FTIR analysis revealed that the phyto-compounds of the fruit extract may be responsible for the production and stabilization of Ag/AgCl NPs. Also, the characterization of the synthesized Ag/AgCl NPs was performed by XRD, TEM, FESEM, and EDS analysis. Finally, the design of a new colorimetric sensor for the efficient distinction and identification of clindamycin and Fe^{3+} ions via phyto-synthesized Ag/AgCl NPs was done. The proposed method has eminent advantages including no pretreatment or derivatization, simplicity, high sensitivity, specificity, and analytical efficiency. This novel method can be used in the throughput analysis of clindamycin (in capsules and injection ampoules) and Fe^{3+} ions (in water samples).

Supplementary Information

The online version contains supplementary material available at https://doi.org/10.1186/s40543-022-00318-5.

Additional file 1: The following seven figures were included in supporting information which is available on journal home. **Figure S1**. Chemical structure of Clindamycin. **Figure S2**. Effect of (a) reaction pH and (b) reaction time on clindamycin colorimetric assay. **Figure S3**. The linear calibration curve of clindamycin. **Figure S4**. (a) The absorption spectrum of the synthesized Ag/AgCl NPs in the presence of some conventional drugs with similar concentrations and (b) their respective color photographs. **Figure S5**. (a) The absorption spectra of the diluted Ag/AgCl NPs solution and (b) its photographic images in the presence of various metal ions. Figure S6 (a) Effect of reaction pH and (b) reaction time on Fe^{3+} ion colorimetric assay. Figure S7 The linear calibration curve of Fe^{3+} ion.

Acknowledgements

The authors thank the Hormozgan University for support of this work.

Authors' contributions

FS as the principal investigator, was the supervisor of the team in all research steps including data gathering, data analysis, and manuscript preparation/revision. AE, as the first author, has the main role for experimental data collection, and FS, EE, and SY contributed to some parts of the experimental data gathering, preparation of results, and data analysis. FS wrote the main manuscript text, and all authors had contributed to the correction and revision of the final version. All authors read and approved the final manuscript.

Funding

This work was supported by Hormozgan University Research Council.

Availability of data and materials

Almost all details of experimental data are presented in the article or additional file and more may be available from the corresponding author via a logical request.

Declarations

Ethics approval and consent to participate

The manuscript does not contain clinical or trial studies on patients, humans, or animals.

Competing interests

The authors declare that they have no competing interests.

Author details

[1]Department of Chemistry, Faculty of Sciences, University of Hormozgan, P.O. Box 3995, Bandar Abbas, Iran. [2]Nanoscience, Nanotechnology and Advanced Materials Research Center, University of Hormozgan, Bandar Abbas, Iran. [3]Molecular Medicine Research Center, Hormozgan Health Institute, Hormozgan University of Medical Sciences, Bandar Abbas, Iran. [4]Research Center

for Health Sciences, Institute of Health, Department of Occupational Health Engineering, School of Health, Shiraz University of Medical Sciences, Shiraz, Iran.

Received: 21 July 2021 Accepted: 14 March 2022
Published online: 29 March 2022

References

Abbaspour A, Mehrgardi MA, Noori A, Kamyabi MA, Khalafi-Nezhad A, Soltani Rad MN. Speciation of iron(II), iron(III) and full-range pH monitoring using paptode: a simple colorimetric method as an appropriate alternative for optodes. Sens Actuat B Chem. 2006;113(2):857–65.

Al-Aboody MS. Silver/silver chloride (Ag/AgCl) nanoparticles synthesized from *Azadirachta indica* lalex and its antibiofilm activity against fluconazole resistant *Candida tropicalis*. Artif Cells Nanomed Biotechnol. 2019;47(1):2107–13.

Ali I, Alharbi OML, ALOthman ZA, Alwarthan A, Al-Mohaimeed AM. Preparation of a carboxymethylcellulose-iron composite for uptake of atorvastatin in water. Int J Biol Macromol. 2019a;132:244–53.

Ali I, Alharbi OML, Alothman ZA, Alwarthan A. Facile and eco-friendly synthesis of functionalized iron nanoparticles for cyanazine removal in water. Colloids Surf B Biointerfaces. 2018a;171:606–13.

Ali I, Alharbi OML, Alothman ZA, Badjah AY. Kinetics, thermodynamics, and modeling of amido black dye photodegradation in water using Co/TiO2 nanoparticles. Photochem Photobiol. 2018b;94(5):935–41. https://doi.org/10.1111/php.12937.

Ali I, Burakov AE, Melezhik AV, Babkin AV, Burakova IV, Neskomornaya MEA, et al. Removal of copper(II) and zinc(II) ions in water on a newly synthesized polyhydroquinone/graphene nanocomposite material: kinetics. Thermodyn Mech Chem. 2019b;4(43):12708–18. https://doi.org/10.1002/slct.201902657.

Ali I, Kon'kova T, Kasianov V, Rysev A, Panglisch S, Mbianda XY, et al. Preparation and characterization of nano-structured modified montmorillonite for dioxidine antibacterial drug removal in water. J Mol Liq. 2021;331:115770.

Aydin FA, Soylak M. Separation, preconcentration and inductively coupled plasma-mass spectrometric (ICP-MS) determination of thorium(IV), titanium(IV), iron(III), lead(II) and chromium(III) on 2-nitroso-1-naphthol impregnated MCI GEL CHP20P resin. J Hazard Mater. 2010;173(1–3):669–74.

Azarudeen RMST, Govindarajan M, AlShebly MM, AlQahtani FS, Amsath A, Senthilmurugan S, et al. Size-controlled biofabrication of silver nanoparticles using the *Merremia emarginata* leaf extract: toxicity on *Anopheles stephensi*, *Aedes aegypti* and *Culex quinquefasciatus* (Diptera: Culicidae) and non-target mosquito predators. J Asia Pac Entomol. 2017;20(2):359–66.

Bajpai M, Pande A, Tewari SK, Prakash D. Phenolic contents and antioxidant activity of some food and medicinal plants. Int J Food Sci Nutr. 2005;56(4):287–91.

Barazandeh Tehrani M, Namadchian M, Fadaye Vatan S, Souri E. Derivative spectrophotometric method for simultaneous determination of clindamycin phosphate and tretinoin in pharmaceutical dosage forms. DARU J Pharm Sci. 2013;21(1):29–35.

Baruah U, Chowdhury D. Functionalized graphene oxide quantum dot–PVA hydrogel: a colorimetric sensor for Fe^{2+}, Co^{2+} and Cu^{2+} ions. Nanotechnology. 2016;27(14):145501–16.

Basiri S, Mehdinia A, Jabbari A. A sensitive triple colorimetric sensor based on plasmonic response quenching of green synthesized silver nanoparticles for determination of Fe^{2+}, hydrogen peroxide, and glucose. Colloids Surf A Physicochem Eng Asp. 2018;545:138–46.

Bitencourt PER, Ferreira LM, Cargnelutti LO, Denardi L, Boligon A, Fleck M, et al. A new biodegradable polymeric nanoparticle formulation containing *Syzygium cumini*: phytochemical profile, antioxidant and antifungal activity and in vivo toxicity. Ind Crops Prod. 2016;83:400–7.

Bitencourt P, Cargnelutti L, Stein C, Lautenchleger R, Ferreira L, Sangoi M, et al. Anti-inflammatory action of seed extract and polymeric nanoparticles of *Syzygium cumini* in diabetic rats infected with *Candida albicans*. J Appl Pharm Sci 2017;007–16.

Chen P-S, Li J-H, Liu T-Y, Lin T-C. Folk medicine *Terminalia catappa* and its major tannin component, punicalagin, are effective against bleomycin-induced genotoxicity in Chinese hamster ovary cells. Cancer Lett. 2000;152(2):115–22.

Chyau C-C, Ko P-T, Mau J-L. Antioxidant properties of aqueous extracts from *Terminalia catappa* leaves. LWT Food Sci Technol. 2006;39(10):1099–108.

da Silva Ferreira V, ConzFerreira ME, Lima LMTR, Frasés S, de Souza W, Sant'Anna C. Green production of microalgae-based silver chloride nanoparticles with antimicrobial activity against pathogenic bacteria. Enzyme Microb Technol. 2017;97:114–21.

Dedić M, Bečić E, Imamović B, Žiga N. Determination of clindamycin hydrochloride content in 1% clindamycin lotion. Bull Chem Technol Bosnia Herzegovina. 2018;50:49–54.

Devi TB, Ahmaruzzaman M. Bio-inspired sustainable and green synthesis of plasmonic Ag/AgCl nanoparticles for enhanced degradation of organic compound from aqueous phase. Environ Sci Pollut Res. 2016;23(17):17702–14. https://doi.org/10.1007/s11356-016-6945-1.

Devi TB, Ahmaruzzaman M, Begum S. A rapid, facile and green synthesis of Ag@AgCl nanoparticles for the effective reduction of 2,4-dinitrophenyl hydrazine. New J Chem. 2016a;40(2):1497–506.

Devi TB, Begum S, Ahmaruzzaman M. Photo-catalytic activity of Plasmonic Ag@AgCl nanoparticles (synthesized via a green route) for the effective degradation of Victoria Blue B from aqueous phase. J Photochem Photobiol B Biol. 2016b;160:260–70.

Durán N, Cuevas R, Cordi L, Rubilar O, Diez MC. Biogenic silver nanoparticles associated with silver chloride nanoparticles (Ag@AgCl) produced by laccase from *Trametes versicolor*. Springerplus. 2014;3(1):645–51.

El-Yazbi FA, Blaih SM. Spectrophotometric and titrimetric determination of clindamycin hydrochloride in pharmaceutical preparations. Analyst. 1993;118(5):577–9.

Eugenio M, Müller N, Frasés S, Almeida-Paes R, Lima LMTR, Lemgruber L, et al. Yeast-derived biosynthesis of silver/silver chloride nanoparticles and their antiproliferative activity against bacteria. RSC Adv. 2016;6(12):9893–904.

Faizi MSH, Gupta S, Mohan KV, Jain VK, Sen P. Highly selective visual detection of Fe^{3+} at ppm level. Sens Actuators B Chem. 2016;222:15–20.

Feizi S, Taghipour E, Ghadam P, Mohammadi P. Antifungal, antibacterial, antibiofilm and colorimetric sensing of toxic metals activities of eco friendly, economical synthesized Ag/AgCl nanoparticles using Malva Sylvestris leaf extracts. Microb Pathog. 2018;125:33–42.

Gao X, Lu Y, He S, Li X, Chen W. Colorimetric detection of iron ions (III) based on the highly sensitive plasmonic response of the N-acetyl-l-cysteine-stabilized silver nanoparticles. Anal Chim Acta. 2015;879:118–25.

Girondi NG, Barreto F, Pigatto MC, Dalla Costa T. Sensitive analytical method to quantify clindamycin in plasma and microdialysate samples: application in a preclinical pharmacokinetic study. J Pharm Biomed Anal. 2018;153:57–62.

Gong C-P, Li S-C, Wang R-Y. Development of biosynthesized silver nanoparticles based formulation for treating wounds during nursing care in hospitals. J Photochem Photobiol B Biol. 2018;183:137–41.

Gopinath V, Priyadarshini S, Meera Priyadharsshini N, Pandian K, Velusamy P. Biogenic synthesis of antibacterial silver chloride nanoparticles using leaf extracts of *Cissus quadrangularis* Linn. Mater Lett. 2013;91:224–7.

Habib IHI, Rizk MS, El-Aryan TR. Determination of clindamycin in dosage forms and biological samples by adsorption stripping voltammetry with carbon paste electrode. Pharm Chem J. 2011;44(12):705–10.

Hadi M, Honarmand E. Application of anodized edge-plane pyrolytic graphite electrode for analysis of clindamycin in pharmaceutical formulations and human urine samples. Russ J Electrochem. 2017;53(4):380–90.

Han S-H, Liu H-M, Sun C-C, Jin P-J, Chen Y. Photocatalytic performance of AgCl@Ag core–shell nanocubes for the hexavalent chromium reduction. J Mater Sci. 2018;53(17):12030–9. https://doi.org/10.1007/s10853-018-2478-y.

Hu X, Pan D, Lin M, Han H, Li F. Graphene oxide-assisted synthesis of bismuth nanosheets for catalytic stripping voltammetric determination of iron in coastal waters. Microchim Acta. 2016;183(2):855–61.

Ibrahim F, El-Deen AK, El Abass SA, Shimizu K. An ecofriendly green liquid chromatographic method for simultaneous determination of nicotinamide and clindamycin phosphate in pharmaceutical gel for acne treatment. J Food Drug Anal. 2017;25(3):741–7.

Khan NA, Ahmed S, Farooqi IH, Ali I, Vambol V, Changani F, et al. Occurrence, sources and conventional treatment techniques for various antibiotics present in hospital wastewaters: a critical review. TrAC Trends Anal Chem. 2020;129:115921.
Kinoshita S, Inoue Y, Nakama S, Ichiba T, Aniya Y. Antioxidant and hepatoprotective actions of medicinal herb, *Terminalia catappa* L. from Okinawa Island and its tannin corilagin. Phytomedicine. 2007;14(11):755–62.
Kowalski P, Konieczna L, Olędzka I, Plenis A, Bączek T. Development and validation of electromigration technique for the determination of lincomycin and clindamycin residues in poultry tissues. Food Anal Methods. 2014;7(2):276–82.
Kulkarni AA, Bhanage BM. Ag@AgCl nanomaterial synthesis using sugar cane juice and its application in degradation of azo dyes. ACS Sustain Chem Eng. 2014;2(4):1007–13.
Li J, Wang X, Huo D, Hou C, Fa H, Yang M, et al. Colorimetric measurement of Fe^{3+} using a functional paper-based sensor based on catalytic oxidation of gold nanoparticles. Sens Actuators B Chem. 2017;242:1265–71.
Liang X, Du L, Su F, Parekh HS, Su W. The application of quantitative NMR for the facile, rapid and reliable determination of clindamycin phosphate in a conventional tablet formulation. Magn Reson Chem. 2014;52(4):178–82.
Liu Y-M, Shi Y-M, Liu Z-L, Peng L-F. Sensitive determination of tilmicosin, erythromycin ethylsuccinate and clindamycin by CE with electrochemiluminescence detection using azithromycin as internal standard and its applications. J Sep Sci. 2010;33(9):1305–11.
Lombi E, Donner E, Taheri S, Tavakkoli E, Jämting ÅK, McClure S, et al. Transformation of four silver/silver chloride nanoparticles during anaerobic treatment of wastewater and post-processing of sewage sludge. Environ Pollut. 2013;176:193–7.
Manivel P, Ilanchelian M. Selective and sensitive colorimetric detection of Hg^{2+} at wide pH range using green synthesized silver nanoparticles as probe. J Clust Sci. 2017;28(3):1145–62.
Mehta VN, Kailasa SK, Wu H-F. Sensitive and selective colorimetric sensing of Fe^{3+} ion by using p-amino salicylic acid dithiocarbamate functionalized gold nanoparticles. New J Chem. 2014;38(4):1503–11.
Mittal AK, Bhaumik J, Kumar S, Banerjee UC. Biosynthesis of silver nanoparticles: elucidation of prospective mechanism and therapeutic potential. J Colloid Interface Sci. 2014;415:39–47.
Mulvaney P. Surface plasmon spectroscopy of nanosized metal particles. Langmuir. 1996;12(3):788–800.
Narayanan KB, Han SS. Highly selective and quantitative colorimetric detection of mercury(II) ions by carrageenan-functionalized Ag/AgCl nanoparticles. Carbohydr Polym. 2017;160:90–6.
Nikaeen G, Yousefinejad S, Rahmdel S, Samari F, Mahdavinia S. Central composite design for optimizing the biosynthesis of silver nanoparticles using plantago major extract and investigating antibacterial, antifungal and antioxidant activity. Sci Rep. 2020;10(1):9642.
Pandya A, Sutariya PG, Lodha A, Menon SK. A novel calix[4]arene thiol functionalized silver nanoprobe for selective recognition of ferric ion with nanomolar sensitivity via DLS selectivity in human biological fluid. Nanoscale. 2013;5(6):2364–71.
Patil MP, Palma J, Simeon NC, Jin X, Liu X, Ngabire D, et al. Sasa borealis leaf extract-mediated green synthesis of silver–silver chloride nanoparticles and their antibacterial and anticancer activities. New J Chem. 2017;41(3):1363–71.
Patil Shriniwas P. Antioxidant, antibacterial and cytotoxic potential of silver nanoparticles synthesized using terpenes rich extract of *Lantana camara* L. leaves. Biochem Biophys Rep. 2017;10:76–81.
Paul P, Duchateau T, van de Griend CS, Adams E, van Schepdael A. Capillary electrophoresis with capacitively coupled contactless conductivity detection method development and validation for the determination of azithromycin, clarithromycin, and clindamycin. J Sep Sci. 2017;40(17):3535–44. https://doi.org/10.1002/jssc.201700560.
Pereira MN, Matos BN, Gratieri T, Cunha-Filho M, Gelfuso GM. Development and validation of a simple chromatographic method for simultaneous determination of clindamycin phosphate and rifampicin in skin permeation studies. J Pharm Biomed Anal. 2018;159:331–40.
Prasad R, Swamy VS. Antibacterial activity of silver nanoparticles synthesized by bark extract of *Syzygium cumini*. J Nanoparticles. 2013;2013:431218–23.
Qin C, Cheng Y, Wang L, Jing X, Wang F. Phosphonate-functionalized polyfluorene as a highly water-soluble iron(III) chemosensor. Macromolecules. 2008;41(21):7798–804.
Rajan R, Chandran K, Harper SL, Yun S-I, Kalaichelvan PT. Plant extract synthesized silver nanoparticles: an ongoing source of novel biocompatible materials. Ind Crops Prod. 2015;70:356–73.
Rautela A, Rani J, Debnath Das M. Green synthesis of silver nanoparticles from *Tectona grandis* seeds extract: characterization and mechanism of antimicrobial action on different microorganisms. J Anal Sci Technol. 2019;10(1):5. https://doi.org/10.1186/s40543-018-0163-z.
Samari F, Baluchi L, Salehipoor H, Yousefinejad S. Controllable phytosynthesis of cupric oxide nanoparticles by aqueous extract of *Capparis spinosa* (caper) leaves and application in iron sensing. Microchem J. 2019;150:104158.
Samari F, Salehipoor H, Eftekhar E, Yousefinejad S. Low-temperature biosynthesis of silver nanoparticles using mango leaf extract: catalytic effect, antioxidant properties, anticancer activity and application for colorimetric sensing. New J Chem. 2018;42(19):15905–16.
Saware K, Venkataraman A. Biosynthesis and characterization of stable silver nanoparticles using ficus religiosa leaf extract: a mechanism perspective. J Clust Sci. 2014;25(4):1157–71.
Schnell S, Ratering S, Jansen K-H. Simultaneous determination of iron(III), iron(II), and manganese(II) in environmental samples by ion chromatography. Environ Sci Technol. 1998;32(10):1530–7.
Shamspur T, Sheikhshoaie I, Mashhadizadeh MH. Flame atomic absorption spectroscopy (FAAS) determination of iron(III) after preconcentration on to modified analcime zeolite with 5-((4-nitrophenylazo)-N-(2′,4′-dimethoxyphenyl))salicylaldimine by column method. J Anal Spectrom. 2005;20(5):476–8.
Shao X, Xie X, Liu Y, Song Z. Rapid determination of clindamycin in medicine with myoglobin–luminol chemiluminescence system. J Pharm Biomed Anal. 2006;41(2):667–70.
Sharmila G, Muthukumaran C, Sandiya K, Santhiya S, Pradeep RS, Kumar NM, et al. Biosynthesis, characterization, and antibacterial activity of zinc oxide nanoparticles derived from Bauhinia tomentosa leaf extract. J Nanostructure Chem. 2018;8(3):293–9. https://doi.org/10.1007/s40097-018-0271-8.
Singh S, Kumar N, Kumar M, Agarwal A, Mizaikoff B. Electrochemical sensing and remediation of 4-nitrophenol using bio-synthesized copper oxide nanoparticles. Chem Eng J. 2017;313:283–92.
Song J, Roh J, Lee I, Jang J. Low temperature aqueous phase synthesis of silver/silver chloride plasmonic nanoparticles as visible light photocatalysts. Dalt Trans. 2013;42(38):13897.
Stalin-Dhas T, Ganesh-Kumar V, Karthick V, Jini-Angel K, Govindaraju K. Facile synthesis of silver chloride nanoparticles using marine alga and its antibacterial efficacy. Spectrochim Acta Part A Mol Biomol Spectrosc. 2014;120:416–20.
Stanković M, Savić V, Marinković V. Determination of clindamycin phosphate in different vaginal gel formulations by reverse phase high performance liquid chromatography. Acta Fac Medicae Naissensis. 2013;30(2):63–71.
Szultka-Mlynska M, Pomastowski P, Buszewski B. Application of solid phase microextraction followed by liquid chromatography-mass spectrometry in the determination of antibiotic drugs and their metabolites in human whole blood and tissue samples. J Chromatogr B. 2018;1086:153–65.
Tahir K, Nazir S, Li B, Khan AU, Khan ZUH, Ahmad A, et al. An efficient photo catalytic activity of green synthesized silver nanoparticles using Salvadora persica stem extract. Sep Purif Technol. 2015;150:316–24.
Tavallali H, Deilamy-Rad G, Parhami A, Mousavi SZ. A novel development of dithizone as a dual-analyte colorimetric chemosensor: detection and determination of cyanide and cobalt (II) ions in dimethyl sulfoxide/water media with biological applications. J Photochem Photobiol B Biol. 2013;125:121–30.
Tripathy A, Raichur AM, Chandrasekaran N, Prathna TC, Mukherjee A. Process variables in biomimetic synthesis of silver nanoparticles by aqueous extract of *Azadirachta indica* (Neem) leaves. J Nanoparticle Res. 2010;12(1):237–46.
Tripathy SK, Woo JY, Han C-S. Colorimetric detection of Fe(III) ions using label-free gold nanoparticles and acidic thiourea mixture. Sens Actuators B Chem. 2013;181:114–8.
Vallejos S, Muñoz A, García FC, Colleoni R, Biesuz R, Alberti G, et al. Colorimetric detection, quantification and extraction of Fe(III) in water by

acrylic polymers with pendant Kojic acid motifs. Sens Actuators B Chem. 2016;233:120–6.
Vanaja M, Gnanajobitha G, Paulkumar K, Rajeshkumar S, Malarkodi C, Annadurai G. Phytosynthesis of silver nanoparticles by Cissus quadrangularis: influence of physicochemical factors. J Nanostructure Chem. 2013;3(1):17.
van der Zee HH, Boer J, Prens EP, Jemec GBE. The effect of combined treatment with oral clindamycin and oral rifampicin in patients with hidradenitis suppurativa. Dermatology. 2009;219(2):143–7.
Villanueva-Ibáñez M, Yañez-Cruz MG, Álvarez-García R, Hernández-Pérez MA, Flores-González MA. Aqueous corn husk extract—mediated green synthesis of AgCl and Ag nanoparticles. Mater Lett. 2015;152:166–9.
Wahba MEK, El-Enany N, Belal F. Application of the Stern–Volmer equation for studying the spectrofluorimetric quenching reaction of eosin with clindamycin hydrochloride in its pure form and pharmaceutical preparations. Anal Methods. 2015;7(24):10445–51.
Wang P, Huang B, Qin X, Zhang X, Dai Y, Wei J, et al. Ag@AgCl: a highly efficient and stable photocatalyst active under visible light. Angew Chemie Int Ed. 2008;47(41):7931–3. https://doi.org/10.1002/anie.200802483.
Wang N, Wang Y, Guo T, Yang T, Chen M, Wang J. Green preparation of carbon dots with papaya as carbon source for effective fluorescent sensing of Iron (III) and *Escherichia coli*. Biosens Bioelectron. 2016;85:68–75.
Wong A, Razzino CA, Silva TA, Fatibello-Filho O. Square-wave voltammetric determination of clindamycin using a glassy carbon electrode modified with graphene oxide and gold nanoparticles within a crosslinked chitosan film. Sens Actuators B Chem. 2016;231:183–93.
Wu S-P, Chen Y-P, Sung Y-M. Colorimetric detection of Fe^{3+} ions using pyrophosphate functionalized gold nanoparticles. Analyst. 2011;136(9):1887.
Yang N, Li WH. Mango peel extract mediated novel route for synthesis of silver nanoparticles and antibacterial application of silver nanoparticles loaded onto non-woven fabrics. Ind Crops Prod Elsevier BV. 2013;48:81–8.
Zhao X, Zhang J, Wang B, Zada A, Humayun M. Biochemical synthesis of Ag/AgCl nanoparticles for visible-light-driven photocatalytic removal of colored dyes. Materials (Basel). 2015;8(5):2043–53.

Publisher's Note